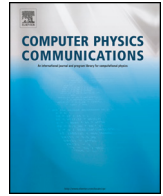




ELSEVIER

Contents lists available at ScienceDirect

Computer Physics Communications

journal homepage: www.elsevier.com/locate/cpc

Computer Programs in Physics

 ULYSSES, universal LeptogeneSiS equation solver: Version 2 [☆], ^{☆☆}

 A. Granelli ^{a,b}, C. Leslie ^c, Y.F. Perez-Gonzalez ^c, H. Schulz ^d, B. Shuve ^e, J. Turner ^{c,*},
 R. Walker ^c
^a Dipartimento di Fisica e Astronomia, Università di Bologna, via Irnerio 46, 40126, Bologna, Italy^b INFN, Sezione di Bologna, viale Berti Pichat 6/2, 40127, Bologna, Italy^c Institute for Particle Physics Phenomenology, Durham University, DH1 3LF, Durham, UK^d Arrival Ltd, Beaumont House, Kensington Village, W14 8TS, London, UK^e Harvey Mudd College, 301 Platt Blvd., Claremont, CA 91711, United States

ARTICLE INFO

Article history:

Received 3 February 2023

Received in revised form 2 June 2023

Accepted 16 June 2023

Available online 26 June 2023

Keywords:

Leptogenesis

Type-I seesaw mechanism

Boltzmann equation

Neutrinos

ABSTRACT

ULYSSES is a Python package that calculates the baryon asymmetry produced from leptogenesis in the context of a type-I seesaw mechanism. In this release, the new features include code which solves the Boltzmann equations for low-scale leptogenesis; the complete Boltzmann equations for thermal leptogenesis applying proper quantum statistics without assuming kinetic equilibrium of the right-handed neutrinos; and, primordial black hole-induced leptogenesis. ULYSSES version 2 has the added functionality of a pre-provided script for a two-dimensional grid scan of the parameter space. As before, the emphasis of the code is on user flexibility, rapid evaluation and is publicly available at <https://github.com/earlyuniverse/ulysses>.

Program summary

Program Title: ULYSSES

CPC Library link to program files: <https://doi.org/10.17632/rzd24f34h2.2>Developer's repository link: <https://github.com/earlyuniverse/ulysses/tree/master/ulysses>

Licensing provisions: MIT

Programming language: Python3

Journal reference of previous version: Comput. Phys. Commun. 262 (2021) 107813

Does the new version supersede the previous version?: Yes

Reasons for the new version: Inclusion of additional effects in Boltzmann equations.

Summary of revisions: Low scale leptogenesis, PBH-induced leptogenesis, and complete leptogenesis equations (non-momentum integrated equations) are provided.

Nature of problem: Solve the Boltzmann equations for thermal, resonant and low-scale leptogenesis through a set of coupled ordinary differential equations.

Solution method: Boltzmann equations are solved using a combination of odeint and solve_ivp in Python3.

© 2023 The Authors. Published by Elsevier B.V. This is an open access article under the CC BY license (<http://creativecommons.org/licenses/by/4.0/>).

1. Introduction

Since its initial proposal [1], leptogenesis has been one of the most well-studied mechanisms to explain matter-antimatter asymmetry. An appealing additional aspect of this mechanism is its connection with neutrino masses and mixing. ULYSSES [2] is a Python package that solves the semi-classical Boltzmann equations (BEs) for leptogenesis in the context of a type-I seesaw mechanism [3–9]. ULYSSES version 1, presented in Ref. [2], provided code for solving the momentum-averaged BEs relevant to leptogenesis based on the out-of-

[☆] The review of this paper was arranged by Prof. Z. Was.

^{☆☆} This paper and its associated computer program are available via the Computer Physics Communications homepage on ScienceDirect (<http://www.sciencedirect.com/science/journal/00104655>).

* Corresponding author.

E-mail address: jessica.turner@durham.ac.uk (J. Turner).

Table 1

The combinations of assumptions used for each case where \checkmark denotes when the assumption is applied and \times when it is neglected.

	Maxwell Boltzmann statistics	RHN Kinetic Equilibrium
Case 1	\checkmark	\checkmark
Case 2	\checkmark	\times
Case 3	\times	\checkmark
Case 4	\times	\times

equilibrium decays of right-handed neutrinos (RHNs) for both resonant and non-resonant regimes. In addition, effects such as lepton flavour, scatterings and spectator processes are available if the user wishes to apply them. In this updated version, we provide additional BEs codes which solve the “complete” set of thermal leptogenesis BEs [10] that properly accounts for quantum statistics and does not assume kinetic equilibrium for the RHNs. Furthermore, we provide state-of-the-art BEs for low-scale (also known as ARS) leptogenesis via oscillations [11,12] and primordial black hole-induced thermal leptogenesis [13,14].

For a given point in the model parameter space, ULYSSES calculates the final baryon asymmetry (given in terms of the baryon-to-photon ratio, η_B , the baryonic yield, Y_B , and the baryonic density parameter, $\Omega_B h^2$) and plots the lepton asymmetry number density as a function of the evolution parameter. For the user who wishes to undertake a multi-dimensional exploration of the parameter space, we have provided instructions on how to use MULTINEST [15] in combination with ULYSSES in the manual of ULYSSES version 1 [2]. ULYSSES is designed modularly, separating the physics of the baryon asymmetry production from the parameter space exploration. In this paper, we will not recapitulate on the BEs provided in version 1, but present the new features along with the basics of ULYSSES installation and functionality. ULYSSES version 2 applies all of the same conventions (Yukawa matrix parametrisation, Higgs vacuum expectation value, normalisation of number densities) as version 1, and we refer the reader to the previous version for discussion on such matters. Further, we refrain from discussing the different regimes and subtleties of the leptogenesis mechanism and instead refer the reader to recent reviews (see, e.g., Refs. [16,17] and references therein) on various aspects of thermal, resonant and low-scale leptogenesis.

The paper is organised as follows: in Section 2, we describe the new pre-provided BEs and follow in Section 3 with installation instructions. In Section 4, we detail the usage of the ULYSSES version 2: namely, we write how to input the model parameters, introduce the new functionality, (that is, the two-dimensional grid scan of the parameter space), and give specific examples on how to call the new model files and their related example parameter cards. Finally, we make concluding remarks in Section 5.

2. Newly added built-in Boltzmann equations

In this section, we list and discuss the *newly added* BEs that are shipped with ULYSSES version 2. We note that version 2 contains the same BEs as version 1, detailed in the previous manual version. In Section 2.1 and Section 2.2, which discuss the BEs for thermal leptogenesis and leptogenesis via oscillations, standard cosmology is assumed. However, in Section 2.3, non-standard cosmology, including a population of primordial black holes, is included in the evolution of the lepton asymmetry.

2.1. Thermal leptogenesis

The majority of papers in the literature apply the following two assumptions:

1. The phase space distribution functions, f_i , of the particles species involved in leptogenesis, $i = N, \Phi, l$, when in thermal equilibrium, are approximated by a Maxwell-Boltzmann distribution, $f_i^{\text{eq}} = e^{-E_i/T}$. Within the Maxwell-Boltzmann statistics, it is also a good approximation to neglect the quantum Pauli-blocking (Bose-enhancement) factors for fermions (bosons), i.e., $1 - f_i^{\text{eq}} \simeq 1$ ($1 + f_i^{\text{eq}} \simeq 1$).
2. The RHNs are in kinetic equilibrium, $f_N/f_N^{\text{eq}} \approx n_N/n_N^{\text{eq}}$, where n_N^{eq} is the (equilibrium) number density of RHNs.

The effects of dropping these assumptions were studied in detail in Ref. [10].

In Table 1, we show four cases where these assumptions are applied or neglected. For Case 1 – Case 4 only the decays and inverse decays of the RHN are included; however, Ref. [10] outlines how to include the effect of scattering and we relegate the inclusion of such an effect for a future ULYSSES version. In all cases, the initial RHN and lepton asymmetry abundance (N_{B-L}) is set using an array $y0$ in the model files, and the default initial abundance is zero-valued.

Case 1 is simply the standard momentum-averaged, one decaying RHN, single-flavoured BEs in which Maxwell-Boltzmann statistics and RHN kinetic equilibrium are assumed. This is shipped with ULYSSES under the code name `etaB1BE1F.py` and shortcut name `1BE1F` (already included in the first version of the code [2]). The BEs for this simple case are

$$\frac{dN_N}{dz} = -D (N_N - N_N^{\text{eq}}), \quad (1a)$$

$$\frac{dN_{B-L}}{dz} = \epsilon D (N_N - N_N^{\text{eq}}) - W N_{B-L}, \quad (1b)$$

where $z \equiv M_1/T$, M_1 is the mass of the lightest RHN and T is the temperature of the plasma; the quantities N_N^{eq} and N_{B-L} are respectively the number of RHNs (when in thermal equilibrium) and $B - L$ asymmetry in a comoving volume normalised to contain one photon when $z \ll 1$ ¹; D and W are respectively the decay and washout parameters (see, e.g., Refs. [10,18] for specific expressions); and ϵ is the CP-asymmetry parameter.

¹ Considering a Bose-Einstein distribution for photons, our choice of normalisation means that $g_\gamma \zeta(3) T^3 a^3 / \pi^2 = 1$, where a^3 is the comoving volume, $g_\gamma = 2$ are the photon degrees of freedom and ζ is the Riemann zeta function with $\zeta(3) \simeq 1.20$. Adopting this normalisation at $z \ll 1$ within the Maxwell-Boltzmann statistics for RHNs

Case 2 solves the following coupled differential system (Case D2 of Ref. [10]):

$$\frac{\partial f_N}{\partial z} = \frac{z^2 K}{\mathcal{E}_N} \left(e^{-\mathcal{E}_N} - f_N \right), \quad (2a)$$

$$\frac{dN_{B-L}}{dz} = -\frac{z^2 K}{4\zeta(3)} \int_0^\infty dy_l \int_{\left| \frac{4y_l^2 - z^2}{4y_l} \right|}^\infty dy_N \frac{y_N}{\mathcal{E}_N} \left[\frac{4}{3} f_N^{\text{eq}} N_{B-L} - 2\epsilon (f_N - f_N^{\text{eq}}) \right], \quad (2b)$$

where K is the decay parameter, \mathcal{E}_N is the RHN energy normalised to temperature, y_l is the modulus of the three-momentum of species l normalised to temperature, and $f_N^{\text{eq}} = e^{-\mathcal{E}_N}$. As the RHN phase space distribution is not initially integrated over energy, there are two integrals in the second coupled differential equation: the first is over the RHN three-momentum normalised to temperature (y_N); the second is over the three-momentum of the lepton l normalised to temperature (y_l). Since there are two integrations per time step, Case 2 is computationally more expensive than Case 1. We note that f_N is calculated on a grid of y_N and then interpolated to perform this integration. The BE code containing Case 2 is `etab1BE1F_Case2.py` and the shortcut name is `1BE1F_Case2`.

Case 3 solves the following coupled differential system (Case D3 of Ref. [10]):

$$\frac{dN_N}{dz} = \frac{K}{K_2(z)} (N_N - N_N^{\text{eq}}) \int_0^\infty dy_N \frac{y_N}{\mathcal{E}_N} \frac{1}{(e^{\mathcal{E}_N} + 1)} \log \left\{ \frac{\sinh[(\mathcal{E}_N - y_N)/2]}{\sinh[(\mathcal{E}_N + y_N)/2]} \right\}, \quad (3a)$$

$$\begin{aligned} \frac{dN_{B-L}}{dz} = & -\frac{z^2 K}{4\zeta(3)} \int_0^\infty dy_l \int_{\left| \frac{4y_l^2 - z^2}{4y_l} \right|}^\infty dy_N \frac{y_N}{\mathcal{E}_N} \left[\left(f_\Phi + \frac{N_N}{N_N^{\text{eq}}} f_N^{\text{eq}} \right) \left(\frac{4}{3} N_{B-L} + 2\epsilon \right) f_l^{\text{eq}} + \right. \\ & \left. - 2\epsilon \frac{N_N}{N_N^{\text{eq}}} f_N^{\text{eq}} (1 + f_\Phi) \right]. \end{aligned} \quad (3b)$$

In the set of equations given above, quantum statistics are applied, but kinetic equilibrium for the RHN is assumed. The integral on the right-hand side of the first equation has no simple analytic form, and it is necessary to perform the integration numerically. The BE code containing Case 3 is `etab1BE1F_Case3.py`, and the shortcut name is `1BE1F_Case3`.

Case 4 solves the following coupled differential system (Case D4 of Ref. [10]):

$$\frac{\partial f_N}{\partial z} = \frac{z^2 K}{\mathcal{E}_N y_N} \frac{f_N (1 + e^{\mathcal{E}_N}) - 1}{(e^{\mathcal{E}_N} + 1)} \log \left\{ \frac{\sinh[(\mathcal{E}_N - y_N)/2]}{\sinh[(\mathcal{E}_N + y_N)/2]} \right\}, \quad (4a)$$

$$\begin{aligned} \frac{dN_{B-L}}{dz} = & -\frac{z^2 K}{4\zeta(3)} \int_0^\infty dy_l \int_{\left| \frac{4y_l^2 - z^2}{4y_l} \right|}^\infty dy_N \frac{y_N}{\mathcal{E}_N} \left[(f_\Phi + f_N) \left(\frac{4}{3} N_{B-L} + 2\epsilon \right) f_l^{\text{eq}} + \right. \\ & \left. - 2\epsilon f_N (1 + f_\Phi) \right], \end{aligned} \quad (4b)$$

where the quantum statistics have been correctly accounted for, and the kinetic equilibrium of the RHN is not assumed. The BE code containing Case 4 is `etab1BE1F_Case4.py`, and the shortcut name is `1BE1F_Case4`. In Fig. 2.1, we show the solutions of Cases 1 to 4 for weak ($K = 0.1$) and strong ($K = 10$) washout. It is well known that, in the strong washout regime ($K \gg 1$), the set of BEs with the assumption of kinetic equilibrium and Maxwell-Boltzmann statistics provides a solution that is quantitatively similar to that of the complete BEs [10]. In the weak washout regime ($K < 1$) the difference can be up to a factor of ~ 2 , mainly due to using the correct Bose-Einstein equilibrium distribution function for the Higgs boson, substantially enlarging the phase space available for the inverse decay process.

To solve Case 2 to 4, `solve_ivp` is used with Runge-Kutta order 5. Although this method was computationally more expensive than the third-order Runge-Kutta method, it provides much more stable and accurate results. Finally, while the integrations in y_N and y_l formally have infinity as an upper integration boundary, we found that an upper limit of 300 is more than sufficient for larger values, and the distributions function is effectively zero-valued.

2.2. Leptogenesis with GeV-scale right-handed neutrinos

When the RHN masses are at the GeV-scale, the naïve seesaw mechanism predicts that they have Yukawa couplings to the SM leptons and Higgs of the order of $\sim 10^{-7}$ (see, e.g., Ref. [19]). Consequently, the RHNs are expected to be out of equilibrium in the early Universe,

and leptons leads to $N_{N,l}^{\text{eq}} = 1/\zeta(3)$, while a more accurate Fermi-Dirac distribution would give $N_{N,l}^{\text{eq}} = 3/4$ (this discrepancy was also noted in Ref. [10]). As in the first version of the code [2], we adopt the analytical approximation $N_{N,l}^{\text{eq}}(z) \simeq (3/8)z^2 K_2(z)$, $K_n(z)$ being the modified n^{th} Bessel functions of the second kind, to match the Maxwell-Boltzmann statistics at $z \gtrsim 1$ and get the correct normalisation condition when $z \ll 1$.

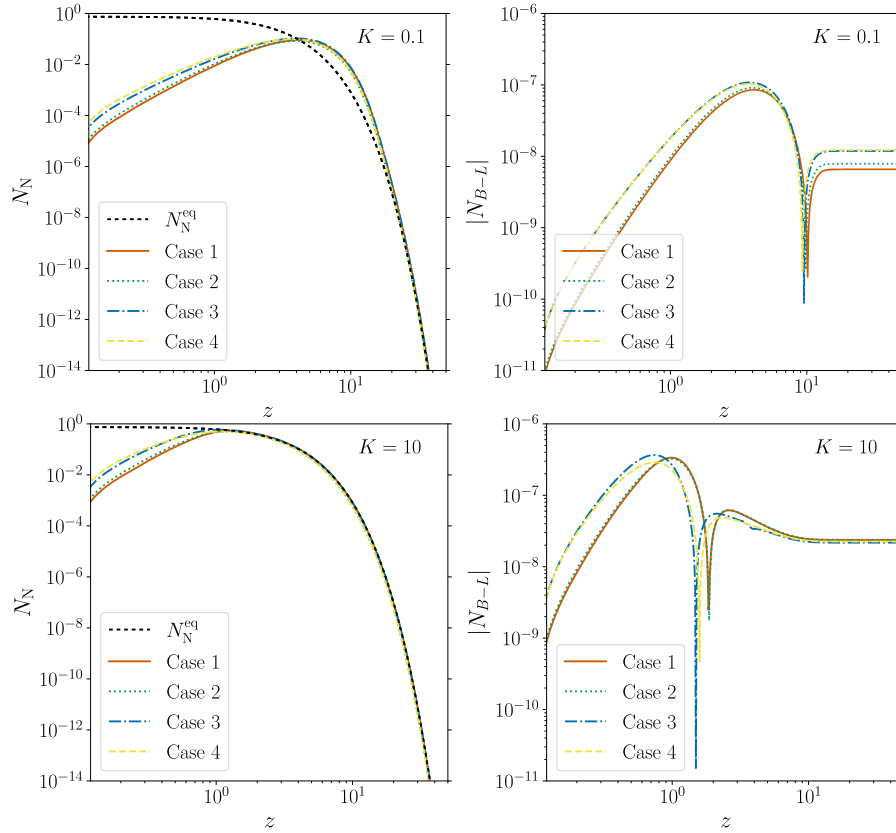


Fig. 2.1. Time evolution of the comoving RHN number density (left) and the absolute value of the lepton asymmetry (right) assuming the decay and CP asymmetry parameter have values $K = 10$ ($K = 0.1$) and $\epsilon = 10^{-6}$ respectively for the top (bottom) panels. Solid/red line denotes Case 1, dotted green Case 2, dotted-dashed blue Case 3 and dashed yellow Case 4. (For interpretation of the colours in the figure(s), the reader is referred to the web version of this article.)

allowing a lepton asymmetry to be generated during their production and approach to equilibrium (“freeze-in”) rather than exclusively during their departure from it (“freeze-out”). This is the Akhmedov-Rubakov-Smirnov (ARS) mechanism for leptogenesis via oscillations of RHNs [11,12]. This mechanism, in which the observed baryon asymmetry can be generated prior to the electroweak phase transition from the dynamics of GeV-scale RHNs, has been extensively studied in recent years (see, e.g., Refs. [19–30]) and has recently received further attention because of its compatibility with couplings of the RHNs to the charged and neutral SM currents that could be accessible at future accelerator and collider experiments [30–33] (for a recent review, see also Ref. [34]), as well as to current and upcoming experiments on charged lepton flavour violating processes involving muons [35–37].

The asymmetry in ARS leptogenesis results from the interplay of CP-violating phases in the RHN Yukawa couplings and oscillation phases among linear combinations of RHN mass eigenstates. Consequently, the semi-classical BE approach to thermal leptogenesis is inadequate as it does not keep track of coherences among states. Instead, the RHN abundances should be modelled as a set of density matrices, and a set of quantum kinetic equations (QKEs) must be solved for the simultaneous evolution of the RHN abundances and lepton flavour asymmetries. SM flavour effects are essential: in the minimal ARS scenario, the initial lepton asymmetry sums to zero over all flavours, and a net baryon asymmetry results only due to subsequent flavour-dependent washout of each flavour asymmetry [11,12].

The QKEs for the RHN density matrices consist of two types of terms: oscillation terms, consisting of commutators of the density matrices with the mass terms in the Hamiltonian (originating from both tree-level and finite-temperature contributions), which account for the oscillation phases; and collision terms, which produce/destroy specific linear combinations of RHN mass eigenstates and also lead to decoherence. Some collision terms are independent of the chemical potentials in SM leptons and allow for the generation of initial lepton flavour asymmetries. In contrast, other terms depend on the lepton chemical potentials and account for back-reactions and washout of the lepton flavour asymmetries.

Since the oscillation phases depend on the momentum of the particular RHN state involved, one must in principle set up QKEs for each RHN momentum mode and separately solve for the asymmetry generated by each mode. This is very computationally intensive and impractical for large-scale studies. Therefore, it is more feasible to instead perform an average over RHN momentum in the oscillation and collision terms and derive QKEs for the momentum-averaged RHN density matrices. Dedicated studies comparing the proper and momentum-averaged treatments typically show agreement up to $\mathcal{O}(1)$ factors (although for individual points the discrepancy can be higher) [28,38]; this level of precision is sufficient for most studies and so we adopt this procedure.²

We implement in ULYSSES the momentum-averaged QKEs relevant to ARS leptogenesis with two RHNs that are quasi-degenerate in mass with masses $M_1 \simeq M_2$, including both lepton-number-conserving (LNC) and lepton-number-violating (LNV) terms. The LNV terms are proportional to the RHN Majorana masses and are consequently suppressed by $M_{1,2}^2/T^2$ relative to the LNV terms for $T \gg M_{1,2}$, but they

² Momentum-dependent asymmetries were also computed in a related model where the oscillating states were produced in the decay of a heavy scalar, with similar conclusions about the accuracy of the momentum averaging procedure [39,40].

can be important for RHN masses close to or above the electroweak scale. The QKEs for ARS leptogenesis have been derived with varying levels of refinement in Refs. [11,12,19,21,22,26,28,30–33,37,41,42]. We adopt a notation similar to that of Ref. [37] (see also Refs. [26,30]), which is physically transparent and correct in the limit of relativistic RHNs, while also admitting a relatively simple approximation for obtaining approximate results beyond the leading expansion in $\mathcal{O}(M_{1,2}^2/T^2)$. The QKEs are written in terms of $(R_N)_{IJ} \equiv (n_N)_{IJ}/n_N^{\text{eq}}$ and $(R_{\bar{N}})_{IJ}$, the RHN and anti-RHN density matrices normalised to the equilibrium abundance, as well as the lepton chemical potentials normalised to the temperature, $\mu_{B/3-L_\alpha}$ and μ_α . More specifically, the quantity μ_α is the reduced chemical potential in the lepton doublet of flavour α , while $\mu_{B/3-L_\alpha}$ parameterises the asymmetry in the anomaly-free charge $B/3 - L_\alpha$ that is conserved by SM interactions (not summed over gauge degrees of freedom in the lepton doublet). Spectator effects relate $\mu_{B/3-L_\alpha}$ and μ_α according to [30]

$$\mu_\alpha = 2 \sum_{\beta} \chi_{\alpha\beta} \mu_{B/3-L_\beta}, \quad (5)$$

$$(\chi_{\alpha\beta}) = -\frac{1}{711} \begin{pmatrix} 257 & 20 & 20 \\ 20 & 257 & 20 \\ 20 & 20 & 257 \end{pmatrix}. \quad (6)$$

The relation to the $B - L$ asymmetry yield (after summing over lepton gauge degrees of freedom) is

$$Y_{B-L} = \sum_{\alpha} \frac{15}{2\pi^2 g_{*,s}} \mu_{B/3-L_\alpha}, \quad (7)$$

where $g_{*,s}$ is the number of entropic degrees of freedom, and the ratio between the baryon and $B - L$ asymmetries is the usual factor of 28/79.

The explicit form of the QKEs we implement is in dimensionless form,

$$\begin{aligned} \frac{T_{\text{ew}}}{M_0} \frac{dR_N}{dz} = & -i \frac{z}{T_{\text{ew}}} [\langle H \rangle, R_N] - \frac{1}{2} \frac{\langle \gamma_N^{(0)} \rangle}{T} \{F^\dagger F, R_N - 1\} + \frac{\langle \gamma_N^{(1)} \rangle}{T} F^\dagger \mu F \\ & - \frac{1}{2} \frac{\langle \gamma_N^{(2)} \rangle}{T} \{F^\dagger \mu F, R_N\} - \frac{z^2}{2T_{\text{ew}}^2} \frac{\langle S_N^{(0)} \rangle}{T} \{MF^T F^* M, R_N - 1\} \\ & - \frac{z^2}{T_{\text{ew}}^2} \frac{\langle S_N^{(1)} \rangle}{T} MF^T \mu F^* M + \frac{z^2}{2T_{\text{ew}}^2} \frac{\langle S_N^{(2)} \rangle}{T} \{MF^T \mu F^* M, R_N\} \\ & - \frac{T_{\text{ew}}}{M_0} \frac{R_N}{Y_N^{\text{eq}}} \frac{dY_N^{\text{eq}}}{dz}, \end{aligned} \quad (8a)$$

$$\begin{aligned} \frac{2\pi^2}{9\zeta(3)} \frac{T_{\text{ew}}}{M_0} \frac{d\mu_{B/3-L_\alpha}}{dz} = & -\frac{1}{2} \frac{\langle \gamma_N^{(0)} \rangle}{T} (FR_N F^\dagger - F^* R_{\bar{N}} F^T)_{\alpha\alpha} + \frac{\langle \gamma_N^{(1)} \rangle}{T} (FF^\dagger)_{\alpha\alpha} \mu_\alpha \\ & - \frac{1}{2} \frac{\langle \gamma_N^{(2)} \rangle}{T} (FR_N F^\dagger + F^* R_{\bar{N}} F^T)_{\alpha\alpha} \mu_\alpha \\ & + \frac{z^2}{2T_{\text{ew}}^2} \frac{\langle S_N^{(0)} \rangle}{T} (F^* MR_N MF^T - FMR_{\bar{N}} MF^\dagger)_{\alpha\alpha} \\ & + \frac{z^2}{T_{\text{ew}}^2} \frac{\langle S_N^{(1)} \rangle}{T} (FM^2 F^\dagger)_{\alpha\alpha} \mu_\alpha \\ & - \frac{z^2}{2T_{\text{ew}}^2} \frac{\langle S_N^{(2)} \rangle}{T} (FMR_{\bar{N}} MF^\dagger + F^* MR_N MF^T)_{\alpha\alpha} \mu_\alpha, \end{aligned} \quad (8b)$$

and the $R_{\bar{N}}$ equation is found by taking $R_N \rightarrow R_{\bar{N}}$, $\mu \rightarrow -\mu$ and $F \rightarrow F^*$ in the QKE for R_N . We define $z \equiv T_{\text{ew}}/T$, $M_0 \equiv M_{\text{Pl}}/(1.66\sqrt{g_{*,s}}) \approx 7.1 \times 10^{17}$ GeV (so that the Hubble rate is $H(T) = T^2/M_0$), μ as the diagonal matrix of lepton doublet chemical potentials μ_α , M as the diagonal matrix of RHN Majorana masses, and $T_{\text{ew}} \approx 131.7$ GeV as the temperature of sphaleron decoupling.³

The thermally averaged Hamiltonian, including both tree-level masses and the effective potential induced by the medium in the high-temperature expansion, is [26,30]

$$\langle H \rangle_{IJ} = \frac{\pi^2 z}{36\zeta(3)T_{\text{ew}}} M_{IJ}^2 + \frac{\pi^2 T_{\text{ew}}}{144\zeta(3)z} (F^\dagger F)_{IJ}, \quad (9)$$

with $I, J = 1, 2$ labelling the zero-temperature RHN mass eigenstates. Given that a multiple of the identity matrix can be added to the Hamiltonian without changing the dynamics (it only leads to an irrelevant overall phase), we subtract the overall mass scale in M^2 , allowing us to replace M^2 with a diagonal matrix with entries $(0, M_2^2 - M_1^2)$. This makes the computations faster as we do not need to keep track of the irrelevant phase given by the overall mass scale.

³ We warn the reader on the different definition we have adopted in this context for the time variable $z = T_{\text{ew}}/T$, while, in the other modules, we have used $z = M_1/T$. We adopt this convention because the asymmetry depends predominantly on the squared mass splitting $M_2^2 - M_1^2$ rather than on the absolute masses $M_{1,2}$, and consequently it is more convenient to normalize to T_{ew} .

The reaction rates (stripped of coupling constants and powers of $M_{1,2}$) are labelled by $\langle \gamma_N^{(j)} \rangle$ for LNC rates and $\langle S_N^{(j)} \rangle$, with $j = 0, 1, 2$, for LNV rates: note that the LNV processes are evaluated in the limit of highly relativistic RHNs and are accompanied in the QKEs with multiplicative powers of $M_{1,2}^2/T^2$, as expected. We perform a thermal average over the momentum-dependent, temperature-normalised rates from Ref. [28].⁴ The rates labelled with $j = 0$ are independent of the lepton chemical potentials, while those corresponding to $j = 1, 2$ depend on lepton chemical potential, with the former being independent of RHN abundances and the latter depending on both lepton chemical potentials and RHN abundances. The ratios $\langle \gamma^{(j)} \rangle/T$ and $\langle S^{(j)} \rangle/T$ are largely independent of the temperature for $T \gg T_{ew}$, and so, by default, ULYSSES fixes these ratios to their values at $T = 10^3$ GeV. However, we have provided an option for the user to include the temperature dependence of these ratios and to take into account higher-order non-relativistic contributions to the LNV terms as in [37]⁵ (further information is provided in Section 4).

The QKEs are solved from a user-specified initial time z_0 to a final time $z = 1$, which is the time of sphaleron decoupling. The user can also specify the initial RHN density matrix at $z = z_0$ in the model file. Two typical choices of initial conditions are $R_N = 0$ and $R_N = 1$, corresponding, respectively, to vanishing or thermal initial conditions; in the latter case, the asymmetry cannot be generated in the freeze-in regime, as there is no initial net production of RHNs given that they start in equilibrium, and the asymmetry only results from the freeze-out mechanism. The default abundance is set to be $R_N = 0$, but can easily be adjusted by the user by changing the y_0 array. Other choices of the initial condition can substantially enhance or decrease the resulting final asymmetry [27,39].

Typically, the QKEs are a stiff system of differential equations because multiple time scales exist corresponding to oscillation and equilibration of the RHNs. Furthermore, the oscillation frequency increases at later times; this can present a challenge to the numerical integration of the QKEs, particularly for earlier onsets of oscillations (equivalent to larger values of $\Delta M_{21}^2 = M_2^2 - M_1^2$). The determination of the asymmetry is simplified by the fact that the generation of lepton flavour asymmetries is suppressed after the onset of rapid oscillations because the positive and negative contributions to the lepton asymmetry average to zero at this point [12], and, consequently, there is little value in tracking the phase information of RHNs past this point. The onset of RHN oscillations occurs around the dimensionless time given by

$$z_{osc} \equiv \left(\frac{12T_{ew}^3}{\Delta M_{21}^2 M_0} \right)^{1/3}. \quad (10)$$

For $z_{osc} > 0.1$, the epoch of rapid oscillations is sufficiently close to the electroweak time $z = 1$ that we solve the full set of QKEs including all oscillations.

For $z_{osc} < 0.1$, we offer the user a “stitching” option to truncate the generation of the flavour asymmetries at a dimensionless time $z_{cut} > z_{osc}$: the full set of QKEs are solved from z_0 to z_{cut} , and the solutions at z_{cut} are used as the initial conditions for a new set of QKEs with the off-diagonal components of R_N and $R_{\bar{N}}$ set to 0 (in the epoch of rapid oscillations the off-diagonal terms all average to zero). This latter set of QKEs is then solved to the final time $z = 1$. The default value of z_{cut} is set to 1, equivalent to solving the full QKEs for the entire time interval relevant for generating the baryon asymmetry. However, the user can specify an alternative value of the stitching time by changing the parameter z_{cut} . This approach allows for rapid integration of the equations for tracking washout effects if the subsequent generation of the asymmetry beyond z_{cut} is known to be small. However, we warn the user that this stitching functionality should only be applied if the necessary condition is met and that an appropriate value of z_{cut} has been selected: for instance, the final result should not change under modest adjustments to z_{cut} , meaning that the full solution has only been truncated when the off-diagonal terms average to zero. Additionally, the user should validate their procedure for a few parameter points by comparing their solution using the stitching option to the full solutions with $z_{cut} = 1$.

Validity and limitations: The QKEs and reaction rates implemented in ULYSSES are expected to be valid for GeV-scale RHNs ($M_{1,2} \ll T_{ew}$) and may give reasonable estimates for somewhat larger masses. However, increasing the RHN masses makes the LNV terms more relevant, and the LNV rates exhibit a pronounced temperature dependence in the vicinity of the electroweak crossover. While our treatment of the QKEs has an option to include this temperature dependence and, to some extent, the non-relativistic contributions for the LNV terms as in Ref. [37], other effects are not currently treated in ULYSSES, such as (more precise) higher-order corrections to the energy-momentum relation and a non-instantaneous treatment of sphaleron decoupling [43]. All these effects become more important for larger RHN masses (especially above 100 GeV) and/or larger coupling (*i.e.*, in the strong washout limit where all the RHNs and SM leptons of each flavour come into equilibrium), and can affect the baryon asymmetry by up to an order of magnitude. In Ref. [32] a somewhat detailed extrapolation of the production rates in the intermediate ($T \sim M$) and non-relativistic ($T \ll M$) regimes is given, taking into account also the effects of the broken electroweak phase at temperature close to the sphaleron decoupling. Interestingly, this allowed the authors of Refs. [31,32] to extend the analysis of leptogenesis with oscillations to scales as large as 10^4 GeV, entering in the regime typically associated to resonant leptogenesis and thus “unifying” the two leptogenesis mechanisms under the same formalism. At the moment, caution is merited when using ULYSSES for RHN masses approaching or exceeding 100 GeV and/or in the strong washout limit, but we aim to implement the aforementioned effects in future versions of the code and allow the user to explore more safely the scenario of leptogenesis with oscillations in such regimes.

2.3. Leptogenesis from primordial black hole evaporation

After discovering Gravitational Waves from Black Hole mergers, analysing the properties and phenomenological effects in Astrophysics and Cosmology of Black Holes has seen a renewed interest. One interesting effect is understanding the possible consequences of Primordial

⁴ The rates from Ref. [28] are provided in tabular form at <http://www.laine.itp.unibe.ch/leptogenesis/>. We thank Stefan Sandner for pointing us towards this electronic database and the public AMIQS code at <https://github.com/stefanmarinus/amiqs> based on Ref. [37]. We have verified that our momentum-averaged reaction rates agree with those from Ref. [37].

⁵ Non-relativistic corrections as in Ref. [37] for the LNC rates are negligible for mass scales below 100 GeV (see, *e.g.*, left panel of Fig. 3 of Ref. [37]), but we still have provided tables for interpolation for the user who wishes to include such corrections.

Black Hole (PBH) evaporation on different particle phenomena in the Early Universe. Leptogenesis indeed can be affected if there existed a non-negligible population of evaporating PBHs [13,14]. Since RHNs would be among the particles emitted by the PBHs, their CP-violating decays could produce more baryon asymmetry than those created in the primordial plasma. Moreover, depending on when the evaporation occurs, the washout effects could be out of equilibrium so that this new population of RHNs would not erase the pre-existing asymmetry. Additionally, if the PBHs had large initial masses, the effect would be different; they inject a large amount of entropy that could dilute the previous lepton asymmetry in the plasma. In order to determine the baryon asymmetry correctly, we need to track in detail the evolution of all Universe components: radiation and PBH energy densities, together with the RHN and $B - L$ number densities.

Kerr PBHs are characterised by their mass M_{BH} and spin parameter $a_* \equiv J/(G^2 M_{\text{BH}}^2) \in [0, 1)$, with J being the BH angular momentum and G the Newton's constant. Due to the emission of Hawking radiation, the PBH mass and spin diminish with the rate given by the following system of coupled equations

$$\frac{dM_{\text{BH}}}{dt} = -F(M_{\text{BH}}, a_*) \frac{1}{G^2 M_{\text{BH}}^2}, \quad (11a)$$

$$\frac{da_*}{dt} = -a_* [G(M_{\text{BH}}, a_*) - 2F(M_{\text{BH}}, a_*)] \frac{1}{G^2 M_{\text{BH}}^3}, \quad (11b)$$

where $F(M_{\text{BH}}, a_*)$ and $G(M_{\text{BH}}, a_*)$, denoted as evaporation functions, contain the dependence on all the degrees of freedom that can be emitted, see Refs. [44–46] for further details. To compute these evaporation functions, we use the code `FRiedmann Solver for Black Hole Evaporation in the Early-universe` `FRISBHEE` [47], whose main library `BHProp.py` is included in `ULYSSES` version 2 for convenience. For further numerical convenience, we consider *grams* as the main units for the PBH mass. The a_* parameter is dimensionless.

To describe in detail the cosmological evolution, we solve the following set of Friedmann equations for the comoving radiation ($\rho_{\text{R}} \equiv a^4 \rho_{\text{R}}$) and PBHs ($\rho_{\text{BH}} \equiv a^3 \rho_{\text{BH}}$) energy densities to be solved together with the BH evolution equations, Eqs. (11),

$$\frac{d\rho_{\text{R}}}{d\xi} = -\frac{F_{\text{SM}}(M_{\text{BH}}, a_*)}{F(M_{\text{BH}}, a_*)} \frac{1}{H} \frac{d \ln M_{\text{BH}}}{dt} a \rho_{\text{BH}}, \quad (12a)$$

$$\frac{d\rho_{\text{BH}}}{d\xi} = \frac{1}{H} \frac{d \ln M_{\text{BH}}}{dt} \rho_{\text{BH}}, \quad (12b)$$

$$H^2 = \frac{8\pi G}{3} (\rho_{\text{BH}} 10^{-3x} + \rho_{\text{R}} 10^{-4x}), \quad (12c)$$

where $\xi \equiv \log_{10}(a/a_0)$ is the logarithm in base 10 of the scale factor a , a_0 the initial scale factor taken to equal 1, H the Hubble rate. Note that we evolve with respect to the dimensionless parameter ξ instead of $z = M_1/T$ since entropy is not conserved throughout the evaporation, and thus we require a different independent variable.

Assuming that the PBH formation occurs in a radiation-dominated era, we have that the initial PBH mass is related to the particle horizon mass as [48]

$$M_{\text{BH}}^{\text{in}} = \frac{4\pi}{3} \gamma \frac{\rho_i}{H_{\text{in}}^3}, \quad (13)$$

with $\gamma = (1/\sqrt{3})^3$ the gravitational collapse factor, and H_{in} the Hubble parameter at the moment of PBH formation. Thus, by fixing the initial PBH mass, we define the initial conditions of the thermal plasma. The initial PBH population is determined in `ULYSSES` via the dimensionless β' parameter, defined as

$$\rho_{\text{BH}}^{\text{in}} = \frac{\beta'}{\gamma^{1/2} - \beta'} \rho_{\text{R}}^{\text{in}} = \frac{\beta'}{\gamma^{1/2} - \beta'} \frac{\pi^2}{30} g_*(T_{\text{in}}) T_{\text{in}}^4, \quad (14)$$

where $\rho_{\text{R}}^{\text{in}}$ corresponds to the initial SM radiation energy density, determined by the initial PBH mass via Eq. (13), using that $H_{\text{in}} \propto T_{\text{in}}^2$ during the initial radiation dominated era. Moreover, in this model, we assume a monochromatic PBH mass distribution, i.e., all black holes possess the same initial mass $M_{\text{BH}}^{\text{in}}$ and spin a_*^{in} . For later convenience, we also consider the explicit evolution of the SM thermal plasma temperature, T

$$\frac{dT}{d\xi} = -\frac{T}{\Delta} \left\{ 1 - \frac{g_*(T)}{g_{*,s}(T)} \frac{1}{4\rho_{\text{R}}} \frac{d\rho_{\text{R}}}{d\xi} \right\}, \quad (15)$$

where Δ describes the change on the effective number of degrees of freedom $g_{*,s}(T)$ in Eq. (12a)

$$\Delta \equiv 1 + \frac{T}{3g_{*,s}(T)} \frac{dg_{*,s}(T)}{dT}. \quad (16)$$

To determine the final baryon-to-photon ratio, we consider the momentum-integrated Boltzmann equations for the comoving thermal (N_N^{TH}) and non-thermal (N_N^{BH}) RHN densities [13,14]

$$\frac{dN_N^{\text{TH}}}{d\xi} = -(N_N^{\text{TH}} - N_N^{\text{eq}}) \frac{\Gamma_N^T}{H}, \quad (17a)$$

$$\frac{dN_N^{\text{BH}}}{d\xi} = -N_N^{\text{BH}} \frac{\Gamma_{N_1}^{\text{BH}}}{H} + N_{\text{BH}} \frac{\Gamma_{\text{BH} \rightarrow N_1}}{H}, \quad (17b)$$

Listing 1: Minimal installation steps.

```
# Installation from within the source tree
git clone https://github.com/earlyuniverse/ulysses.git
cd ulysses
pip install . --user

# Installation with pip or pip3 from pypi.org
pip install ulysses --user
```

Listing 2: Minimal update steps.

```
# Updating installation
pip install ulysses==2.0.3 --user
```

where $\Gamma_{N_1}^T$, $\Gamma_{N_1}^{\text{BH}}$ are the decay widths corrected by an inverse time dilation factor averaged over the plasma and BH temperature, respectively,

$$\Gamma_{N_1}^{\text{T,BH}} \equiv \left\langle \frac{M_1}{E_{N_1}} \right\rangle_{\text{T,BH}} \Gamma_{N_1}, \quad (18)$$

and Γ_{N_1} is the RHN decay width. To address the generation of RHNs from the PBH density, we have included a source term in Eq. (17b) equal to the comoving PBH number density, $N_{\text{BH}} \equiv \rho_{\text{BH}}/M_{\text{BH}}$, times $\Gamma_{\text{BH} \rightarrow N_1}$, the total RHN emission rate per BH; see Ref. [13]. The equation for the $B-L$ asymmetry, N_{B-L} , is

$$\frac{dN_{B-L}}{d\xi} = \frac{\epsilon}{H} \left[(N_N^{\text{TH}} - N_N^{\text{eq}}) \Gamma_{N_1}^T + N_N^{\text{BH}} \Gamma_{N_1}^{\text{BH}} \right] - \frac{1}{H} \left(\frac{1}{2} \Gamma_{N_1}^T N_N^{\text{eq}} + \gamma \right) \frac{N_{B-L}}{N_\ell^{\text{eq}}}, \quad (19)$$

with N_ℓ^{eq} being the lepton equilibrium abundance. The term proportional to N_{B-L} corresponds to the washout processes, including the $\Delta L = 2$ interactions. After obtaining the $B-L$ number density, we similarly obtain η_B as for other leptogenesis scenarios. An important difference with the other models in ULYSSES should be noted here. The RHN neutrino abundances, both equilibrium and out-of-equilibrium, for thermal and PBH sources are normalized with respect to the *initial* photon density, $n_\gamma^{\text{in}} = 2\zeta(3)T_{\text{in}}^3/\pi^2$.

In ULYSSES version 2, we solve the system of equations Eqs. (11), (12), (17), (19) together with the equation for the plasma temperature, Eq. (15). The code containing the mentioned system of equations and their solution is `etabPBH.py`, with the shortcut name being `1BE1F_PBH`, and we provide an example parameter card; details of their usage are found in Section 4. Since the time-evolution equations for the PBH mass and spin become quite stiff when the evaporation enters the final stages, we have implemented an iterative approach to evolve until the PBH mass reaches the Planck Mass, the point at which we stop the evolution. We solve the equations from the initial black hole mass until 1% of the initial value and then take the found solutions as initial conditions for a new iteration. This is done until the PBH mass arrives at the Planck scale. If thermal leptogenesis occurs after the PBH evaporation, we have added a second set of BEs, which is solved using the solutions obtained after properly evolving the PBH particle production. Finally, the user can modify the initial abundances of particles by adjusting the `y0` array in the model file.

We note that PBH-domination forms a very specific non-standard cosmology for leptogenesis. In future versions of ULYSSES, we aim to implement further scenarios of non-standard cosmologies for baryogenesis such as late-time decays of string moduli [49]. We also note that ULYSSES currently includes the module `etab1BE1Fsf.py` in which the evolution is done with respect to the scale factor. Thus, such a module could be used as a basis for the implementation of a specific non-standard cosmology.

3. Installation

The code is hosted on <https://github.com/earlyuniverse/ulysses>. Once the git repository is pulled, the basic installation steps are shown in Listing 1 and Listing 2. In addition, releases are packaged and available to install with `pip` from <https://pypi.org/>.

We note that, if the user has the first installation of ULYSSES, this can be updated to the current version.

3.1. Core dependencies

The code is written in Python3 and heavily uses the widely available modules `NumPy` [50,51] and `SciPy` [52] packages.⁶ We accelerate the computation with the just-in-time compiler provided by `NUMBA` [53] where meaningful. At its core, ULYSSES solves a set of coupled differential equations. To undertake this task we use `solve_ivp` and `odeintw` [54]. The former is a standard Python package for solving initial value problems for ordinary differential equations, while the latter provides a wrapper of `scipy.integrate.odeint` that allows it to handle complex and matrix differential equations; it is redistributed with ULYSSES and does not need to be downloaded separately. These dependencies for ULYSSES are automatically resolved during the install process with `pip`. They provide the minimal functionality for solving Boltzmann equations for a given point in the model parameter space. In ULYSSES version 2, Python packages `TQDM` and `TERMCOLOR` must also be pip-installed.

⁶ We note that outdated versions of `NUMPY` and `SCIPY` may lead to numerical instabilities, especially for `1BE1F_Case2`, `1BE1F_Case3` and `1BE1F_Case4`, and thus we recommend that the user upgrade to the latest, up-to-date versions.

Table 2

Overview of global parameters and their default values. Neutrino mass squared splittings are taken from the central values of NuFIT 5.1 global fit data (without atmospheric data from Super-Kamiokande) [55].

Parameter	Variable name	Default	Unit
Higgs vacuum expectation value, v	vev	174.0	[GeV]
Higgs mass, M_H	mhiggs	125.35	[GeV]
Z boson mass, M_Z	mz	91.1876	[GeV]
Planck mass, M_{Pl}	mplanck	1.22×10^{19}	[GeV]
Neutrino cosmological mass, m_*	mstar	10^{-12}	[GeV]
Degrees of freedom, g_*	gstar	106.75	
Solar mass squared splitting, Δm_{\odot}^2	m2solar	7.42×10^{-23}	[GeV ²]
Atm. mass squared splitting (normal), Δm_{atm}^2	m2atm	2.515×10^{-21}	[GeV ²]
Atm. mass squared splitting (inverted), $\Delta m_{\text{atm,inv}}^2$	m2atminv	2.498×10^{-21}	[GeV ²]

Table 3

Overview of the input parameters in the Casas-Ibarra parametrisation.

Parameter	Unit	Code input example	
δ	[°]	delta	213.70
α_{21}	[°]	a21	81.60
α_{31}	[°]	a31	476.70
θ_{23}	[°]	t23	48.58
θ_{12}	[°]	t12	33.63
θ_{13}	[°]	t13	8.52
x_1	[°]	x1	90.00
y_1	[°]	y1	-120.00
x_2	[°]	x2	87.00
y_2	[°]	y2	0.00
x_3	[°]	x3	180.00
y_3	[°]	y3	-120.00
$\log_{10}(m_{1/3})$	[eV]	m	-1.10
$\log_{10}(M_1)$	[GeV]	M1	12.10
$\log_{10}(M_2)$	[GeV]	M2	12.60
$\log_{10}(M_3)$	[GeV]	M3	13.00

4. Usage of ULYSSES version 2

4.1. The model parameters

All global constants are defined in the `__init__` function of the base class and they are shown in Table 2. We allow the user to set their values via the standard Python keyword argument formalism using the variable names shown in the second column of Table 2. The required input from the user is the set of model parameters which stems from the Casas-Ibarra parametrisation of the Yukawa matrix Y , as shown below [56]:

$$Y = \frac{1}{v} U \sqrt{\hat{m}_\nu} R^T \sqrt{M_R}, \quad (20)$$

where $v = 174 \text{ GeV}$ is the Higgs's vacuum expectation value, U is the 3×3 unitary Pontecorvo-Maki-Nakagawa-Sakata (PMNS) regulating the neutrino (lepton) mixing, $\hat{m}_\nu = \text{diag}(m_1, m_2, m_3)$ is the diagonal light neutrino mass matrix, R is a 3×3 complex orthogonal matrix and $M_R = \text{diag}(M_1, M_2, M_3)$ is the diagonal mass matrix of the RHNs. We apply the Particle Data Group convention [57] to parameterise the PMNS matrix:

$$U = \begin{pmatrix} 1 & 0 & 0 \\ 0 & c_{23} & s_{23} \\ 0 & -s_{23} & c_{23} \end{pmatrix} \begin{pmatrix} c_{13} & 0 & s_{13}e^{-i\delta} \\ 0 & 1 & 0 \\ -s_{13}e^{i\delta} & 0 & c_{13} \end{pmatrix} \begin{pmatrix} c_{12} & s_{12} & 0 \\ -s_{12} & c_{12} & 0 \\ 0 & 0 & 1 \end{pmatrix} \begin{pmatrix} 1 & 0 & 0 \\ 0 & e^{i\frac{\alpha_{21}}{2}} & 0 \\ 0 & 0 & e^{i\frac{\alpha_{31}}{2}} \end{pmatrix}, \quad (21)$$

where $c_{ij} \equiv \cos \theta_{ij}$, $s_{ij} \equiv \sin \theta_{ij}$, δ is the Dirac phase and α_{21} , α_{31} are the Majorana phases [58] which, in general, can vary between $0 \leq \alpha_{21}, \alpha_{31} \leq 2\pi$. The R -matrix can be written in the following form:

$$R = \begin{pmatrix} 1 & 0 & 0 \\ 0 & c_{\omega_1} & s_{\omega_1} \\ 0 & -s_{\omega_1} & c_{\omega_1} \end{pmatrix} \begin{pmatrix} c_{\omega_2} & 0 & s_{\omega_2} \\ 0 & 1 & 0 \\ -s_{\omega_2} & 0 & c_{\omega_2} \end{pmatrix} \begin{pmatrix} c_{\omega_3} & s_{\omega_3} & 0 \\ -s_{\omega_3} & c_{\omega_3} & 0 \\ 0 & 0 & 1 \end{pmatrix}, \quad (22)$$

where $c_{\omega_i} \equiv \cos \omega_i$, $s_{\omega_i} \equiv \sin \omega_i$ and the complex angles are given by $\omega_i \equiv x_i + iy_i$ for x, y free, real parameters. The R -matrix in Eq. (22) have $\det(R) = 1$. Often, in the literature, a phase factor $\varphi = \pm 1$ is included in the definition of certain elements of the matrix R to allow for the both cases $\det(R) = \pm 1$. However, one can extend the range of values of the Majorana phases to $0 \leq \alpha_{21}, \alpha_{31} \leq 4\pi$ to effectively account for both cases of $\det(R) = \pm 1$ and consider, in this way, the same full set of R and Yukawa matrices [59].

The Casas-Ibarra parameters (and their units) may be input by the user in the code and an example is given in Table 3. Specifically, assigning a value to the code variables named `delta`, `a21`, `a31`, `t23`, `t12`, `t13`, `x1`, `y1`, `x2`, `y2`, `x3`, `y3`, `M1`, `M2`, `M3` and `m`, the user

Listing 3: Example of an input parameter card using the Casas-Ibarra parametrisation.

m	-1.10
M1	12.10
M2	12.60
M3	13.00
delta	213.70
a21	81.60
a31	476.70
x1	90.00
x2	87.00
x3	180.00
y1	-120.00
y2	0.00
y3	-120.00
t12	33.63
t13	8.52
t23	49.58

Listing 4: Example of an input parameter card for generic Yukawas and RHN masses.

Y11_mag	0.01
Y12_mag	0.01
Y13_mag	0.01
Y21_mag	0.01
Y22_mag	0.03
Y23_mag	0.05
Y31_mag	0.01
Y32_mag	0.03
Y33_mag	0.05
Y11_phs	-1.11
Y12_phs	2.89
Y13_phs	1.32
Y21_phs	2.88
Y22_phs	-0.23
Y23_phs	-1.80
Y31_phs	-1.72
Y32_phs	2.96
Y33_phs	1.39
M1	12.0
M2	12.5
M3	13.0

fixes, respectively, the PMNS phases and angles in degrees, the real and imaginary parts of the three complex angles of the R -matrix in degrees, the three RHN masses in GeV and of the lightest neutrino mass (that is either m_1 or m_3 , depending on the ordering of the light neutrino masses) in eV. In contrast, the two heavier neutrino masses are fixed at the best-fit values using the global fit data on solar and atmospheric mass squared differences [55], the values of which, if necessary, can be changed directly by the user in `ulsbase.py`. Since the last release, we have updated the neutrino parameters to the NuFIT 5.1 global fit central values [55]. We stress that, as an input, the user fixes the logarithm in base 10 of the masses of the RHNs and the lightest active neutrino. In particular, using the example in Table 3, which is also given separately in Listing 3 in the form of a parameter card, the lightest active neutrino mass is fixed at $m_1 = 10^{-1.1}$ eV and the RHN masses at $M_{1,2,3} = 10^{12.1, 12.6, 13}$ GeV.

The Casas-Ibarra parametrisation is one popular parametrisation of the Yukawa matrix that guarantees the correct prediction of the observed pattern of light neutrino masses and mixing. However, ULYSSES also allows the user to provide their own Yukawa matrix in polar coordinates and calculate the resultant baryon asymmetry. We note that, in the latter option, the user will need to ensure independently that the oscillation data are satisfied. The input logic is such that each element of the Yukawa matrix, Y_{ij} , is determined by two independent parameters Y_{ij_mag} and Y_{ij_phs} , which are the absolute magnitude and phase (the polar coordinates) of the Yukawa entry, respectively:

$$Y_{ij} = Y_{ij_mag} \cdot \exp(i Y_{ij_phs}) . \quad (23)$$

An example input card for a generic Yukawa parametrisation in polar coordinates is shown in Listing 4.

The code for PBH-induced leptogenesis requires the user to specify also the parameters a_* , β' and $M_{\text{BH}}^{\text{in}}$ introduced in Section 2.3. Therefore, the user, in addition to the parameters of the type-I seesaw model described above, needs to fix also the parameters a_* , β' and $M_{\text{BH}}^{\text{in}}$ by assigning a value to each code variables named `aPBHi`, `bPBHi` and `MPBHi` (see further in Section 4.3 for a specific parameter card and related example). `MPBHi` is the initial mass of the black holes in grams (monochromatic mass distribution) in logarithm of base 10, `aPBHi` is the dimensionless parameter related to the spin and takes values between 0 (spinless) and 1 (maximally spinning) and, finally, `bPBHi` is related to the initial number density of black holes (in logarithm of base 10).

4.2. Functionalities

For convenience, we ship four runtime scripts which use the ULYSSES module for the evaluation of η_B at a single point, as well as in one-dimensional and in multi-dimensional parameter space explorations:

- `uls-calc`
- `uls-scan`
- `uls-nest`
- `uls-scan2D`

The first three of the functionalities listed above were already shipped with ULYSSES version 1 [2], while the new functionality shipped with version 2 is `uls-scan2D`, which generalises `uls-scan` to two dimensions. We provide some examples of the usage of the functionalities within ULYSSES version 2 in the next subsections.

4.3. Examples

To display the pre-provided BEs, including those discussed in Section 2, and the strings needed to load them from the command line the user can call:

Listing 5: Example of an input card for ARS leptogenesis (2RHNosc.dat).

```
m -100.
M1 -100.
M2 0.0
M3 4.34294e-9
x1 45.
y1 40.107
x2 0.
y2 0.
x3 0.
y3 0.
delta 221.
a21 322.
a31 0.
t12 33.8486
t13 8.60954
t23 48.5904
```

Listing 6: Example of an input card for ARS leptogenesis where the stitch is required (2RHNosc_examplestitch.dat).

```
m -100.
M1 -100.
M2 0.0
M3 9.34294e-9
x1 45.
y1 40.107
x2 0.
y2 0.
x3 0.
y3 0.
delta 221.
a21 322.
a31 0.
t12 33.8486
t13 8.60954
t23 48.5904
```

```
# display list of available models
uls-models
```

In addition to those BE codes shipped with ULYSSES version 1, we have included new codes with their own “shortcut names”. For the cases of thermal leptogenesis discussed in Section 2.1, the “shortcut names” for Cases 2 to 4 are 1BE1F_Case2, 1BE1F_Case3, 1BE1F_Case4 respectively. An example call to `uls-calc` on 1BE1F_Case4 is shown below:

```
# call 1BE1F_Case4 on input card 1N1F.dat and output 1BE1F_Case4.pdf
uls-calc -m 1BE1F_Case4 examples/1N1F.dat -o 1BE1F_Case4.pdf
```

which returns the baryon asymmetry (in terms of the baryon-to-photon ratio, the baryonic yield and the baryonic density) and a plot (1BE1F_Case4.pdf) showing the time evolution of the lepton asymmetry and baryon-to-photon ratio.

For ARS leptogenesis, there are two modules with shortcut names BEARS and BEARS_INTERP, which use temperature-independent and temperature-dependent rates, respectively. The latter module also takes into account non-relativistic corrections to the LNV rates as detailed in Ref. [37]. An example call for this code is

```
# call ARS BE with temperature independent rates on input card pars.dat
uls-calc -m BEARS examples/2RHNosc.dat
```

where the output displayed on the terminal consists of the Yukawa matrix and baryon asymmetry given in terms of η_B , Y_B and Ω_B . Note that, to use the temperature-dependent rates in the above command, BEARS_INTERP should be used instead of BEARS.

In the above example, the input card is shown in Listing 5. In this case, the mass splittings are very small, and the oscillation length, as discussed in Section 2.2, is $z_{\text{osc}} > 0.1$ and no stitching of the solutions is required. There is a second example card, named 2RHNosc_examplestitch.dat, which has a larger mass squared splitting between the two right-handed neutrinos resulting in $z_{\text{osc}} < 0.1$. The integration time can be longer in this case, so the code allows the user to specify where the stitch should occur:

```
# call BE_ARS on input card pars.dat
uls-calc -m BEARS examples/2RHNosc_examplestitch.dat --zcut 0.6
```

where, in the above case, the cut is chosen to be at $z_{\text{cut}} = 0.6$. The example input card used in the above example is shown in Listing 6. The ARS code also automatically outputs a plot of the absolute magnitudes of the chemical potentials as a function of z .

To call PBH-induced leptogenesis requires an input card not only with the usual Casas-Ibarra parametrisation but also with the PBH parameters (a_* , β' and $M_{\text{BH}}^{\text{in}}$), as detailed in Section 2.3 and Section 4.1. An example input card shipped with ULYSSES version 2 is shown in Listing 7. A code example where a one-dimensional scan in variable x_1 is performed using the parameters of Listing 7 is given below:

```
# call 1BE1F_PBH on input card PBH.dat
uls-scan -m 1BE1F_PBH examples/PBH.dat -o PBHscan.pdf
```

The one-dimensional scan's illustrative output is given in the left panel of Fig. 4.1. An example of applying `uls-scan2D` is given below:

```
# Use one of the built-in plugins
uls-scan2D -m 1BE1F examples/1N1F_2Dscan.dat -o example_2D.pdf
```

Listing 7: Example of an input card (PBH.dat) for the PBH-assisted leptogenesis model.

```

m -0.576754
M1 14.0000
M2 14.4771
M3 14.7785
x1 0.0 90.0
y1 0.
x2 45.0000
y2 25.2495
x3 0.
y3 0.
delta 194.
a21 0.
a31 0.
t12 33.44
t13 8.57
t23 49.2
MPBHi 0.0
aPBHi 0.0
bPBHi -5.68

```

Listing 8: Example of an input parameter card (1N1F_2Dscan.dat) for uls-scan2D using the Casas-Ibarra parametrisation.

```

m -100
M1 14
M2 15
M3 16
x1 180
y1 1.4
x2 0. 45.
y2 0. 45.
x3 180
y3 11
delta 217.
a21 0.
a31 0
t23 49.7
t12 33.82
t13 8.610

```

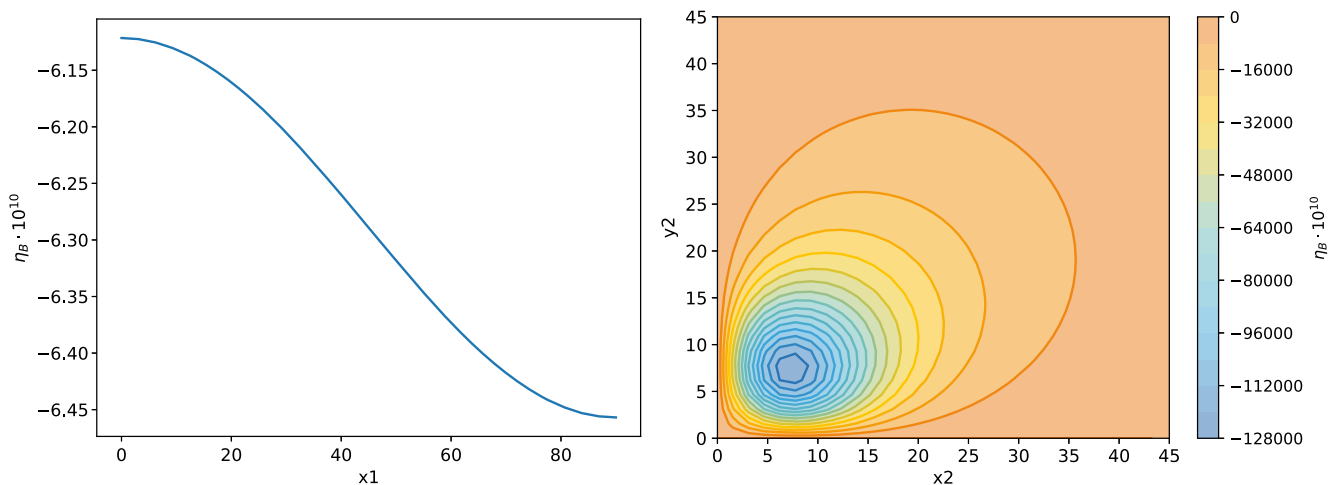


Fig. 4.1. On the left is the one-dimensional scan output of 1BE1F_PBH.py on the parameter card PBH.dat in Listing 7, while on the right is the contour plot output from uls-scan2D using the input card 1N1F_2Dscan.dat in Listing 8.

where the input parameter card 1N1F_2Dscan.dat, shown in Listing 8, let the parameters x_2 and y_2 vary within the range $[0^\circ, 45^\circ]$. The code saves a pdf file depicting a contour plot of $\eta_B \times 10^{10}$ as a function of varied parameters, as shown in the right panel of Fig. 4.1. If the user wishes to obtain a text file with the numerical output, the following command can be used:

```

# Use one of the built-in plugins
uls-scan2D -m 1BE1F examples/1N1F_2Dscan.dat -o example_2D.txt

```

saving in the first and second columns of the output text file the values of the first and second varied parameters, respectively, while in the third column the calculated $\eta_B \times 10^{10}$.

5. Summary and discussion

In this second release of ULYSSES we have implemented the Boltzmann equations for the complete phase-space evolution of thermal leptogenesis, based on the work of Ref. [10], the equations for non-resonant leptogenesis in the context of a primordial black hole dominated early Universe (see Refs. [13,14]) and, finally, the kinetic equations for leptogenesis via oscillations [11,12] based on a notation similar to that of Ref. [37] (see also Refs. [26,30]). The functionality of ULYSSES has been expanded with the facility for a two-dimensional scan. As stated in the first version of the manual [2], we view this as a community project and invite users to add and share their plugins with others. This can be done via issues and pull requests on our GitHub repository.

Declaration of competing interest

The authors declare that they have no known competing financial interests or personal relationships that could have appeared to influence the work reported in this paper.

Data availability

No data was used for the research described in the article.

Acknowledgements

We would like to thank Roberta Calabrese and Serguey T. Petcov for useful feedback on the output of the code for PBH and ARS leptogenesis, respectively, and we would like to thank Stefan Sandner and Dave Tucker-Smith for helpful discussions. This work used the DiRAC@Durham facility managed by the Institute for Computational Cosmology on behalf of the STFC DiRAC HPC Facility (www.dirac.ac.uk). The equipment was funded by BEIS capital funding via STFC capital grants ST/P002293/1, ST/R002371/1 and ST/S002502/1; Durham University and STFC operations grant ST/R000832/1. DiRAC is part of the National e-Infrastructure. This work has made use of the Hamilton HPC Service of Durham University. The work of BS is supported by Research Corporation for Science Advancement through Cottrell Scholar Grant #27632.

References

- [1] M. Fukugita, T. Yanagida, *Phys. Lett. B* 174 (1986) 45.
- [2] A. Granelli, K. Moffat, Y.F. Perez-Gonzalez, H. Schulz, J. Turner, *Comput. Phys. Commun.* 262 (2021) 107813, arXiv:2007.09150.
- [3] P. Minkowski, *Phys. Lett. B* 67 (1977) 421.
- [4] T. Yanagida, *Conf. Proc. C* 7902131 (1979) 95.
- [5] M. Gell-Mann, P. Ramond, R. Slansky, *Conf. Proc. C* 790927 (1979) 315, arXiv:1306.4669.
- [6] S. Glashow, *NATO Adv. Stud. Inst. Ser. B* 61 (1980) 687.
- [7] R.N. Mohapatra, G. Senjanovic, *Phys. Rev. Lett.* 44 (1980) 912.
- [8] J. Schechter, J.W.F. Valle, *Phys. Rev. D* 22 (1980) 2227.
- [9] J. Schechter, J.W.F. Valle, *Phys. Rev. D* 25 (1982) 774.
- [10] F. Hahn-Woernle, M. Plumacher, Y.Y. Wong, *J. Cosmol. Astropart. Phys.* 08 (2009) 028, arXiv:0907.0205.
- [11] E.K. Akhmedov, V.A. Rubakov, A.Y. Smirnov, *Phys. Rev. Lett.* 81 (1998) 1359, arXiv:hep-ph/9803255.
- [12] T. Asaka, M. Shaposhnikov, *Phys. Lett. B* 620 (2005) 17, arXiv:hep-ph/0505013.
- [13] Y.F. Perez-Gonzalez, J. Turner, *Phys. Rev. D* 104 (2021) 103021, arXiv:2010.03565.
- [14] N. Bernal, C.S. Fong, Y.F. Perez-Gonzalez, J. Turner, *Phys. Rev. D* 106 (2022) 035019, arXiv:2203.08823.
- [15] F. Feroz, M.P. Hobson, M. Bridges, *Mon. Not. R. Astron. Soc.* 398 (2009) 1601, arXiv:0809.3437.
- [16] D. Bodeker, W. Buchmuller, *Rev. Mod. Phys.* 93 (2021) 035004, arXiv:2009.07294.
- [17] P. Asadi, et al., Early-universe model building, arXiv:2203.06680.
- [18] W. Buchmüller, P. Di Bari, M. Plumacher, *Ann. Phys.* 315 (2005) 305, arXiv:hep-ph/0401240.
- [19] J. Ghiglieri, M. Laine, *J. High Energy Phys.* 05 (2017) 132, arXiv:1703.06087.
- [20] M. Shaposhnikov, *Nucl. Phys. B* 763 (2007) 49, arXiv:hep-ph/0605047.
- [21] T. Asaka, S. Eijima, H. Ishida, *J. Cosmol. Astropart. Phys.* 02 (2012) 021, arXiv:1112.5565.
- [22] L. Canetti, M. Drewes, T. Frossard, M. Shaposhnikov, *Phys. Rev. D* 87 (2013) 093006, arXiv:1208.4607.
- [23] B. Shuve, I. Yavin, *Phys. Rev. D* 89 (2014) 075014, arXiv:1401.2459.
- [24] P. Hernández, M. Kekic, J. López-Pavón, J. Racker, N. Rius, *J. High Energy Phys.* 10 (2015) 067, arXiv:1508.03676.
- [25] M. Drewes, B. Garbrecht, D. Gueter, J. Klarić, *J. High Energy Phys.* 12 (2016) 150, arXiv:1606.06690.
- [26] P. Hernández, M. Kekic, J. López-Pavón, J. Racker, J. Salvado, *J. High Energy Phys.* 08 (2016) 157, arXiv:1606.06719.
- [27] T. Asaka, S. Eijima, H. Ishida, K. Minogawa, T. Yoshii, *Phys. Rev. D* 96 (2017) 083010, arXiv:1704.02692.
- [28] J. Ghiglieri, M. Laine, *J. High Energy Phys.* 02 (2018) 078, arXiv:1711.08469.
- [29] M. Drewes, B. Garbrecht, P. Hernández, M. Kekic, J. Lopez-Pavon, J. Racker, et al., *Int. J. Mod. Phys. A* 33 (2018) 1842002, arXiv:1711.02862.
- [30] A. Abada, G. Arcadi, V. Domcke, M. Drewes, J. Klarić, M. Lucente, *J. High Energy Phys.* 01 (2019) 164, arXiv:1810.12463.
- [31] J. Klarić, M. Shaposhnikov, I. Timiryasov, *Phys. Rev. Lett.* 127 (2021) 111802, arXiv:2008.13771.
- [32] J. Klarić, M. Shaposhnikov, I. Timiryasov, *Phys. Rev. D* 104 (2021) 055010, arXiv:2103.16545.
- [33] M. Drewes, Y. Georis, J. Klarić, *Phys. Rev. Lett.* 128 (2022) 051801, arXiv:2106.16226.
- [34] E.J. Chun, et al., *Int. J. Mod. Phys. A* 33 (2018) 1842005, arXiv:1711.02865.
- [35] A. Granelli, J. Klarić, S.T. Petcov, Tests of low-scale leptogenesis in charged lepton flavour violation experiments, arXiv:2206.04342.
- [36] K.A.U. Calderón, I. Timiryasov, O. Ruchayskiy, Improved constraints and the prospects of detecting TeV to PeV scale heavy neutral leptons, arXiv:2206.04540.
- [37] P. Hernandez, J. Lopez-Pavon, N. Rius, S. Sandner, *J. High Energy Phys.* 12 (2022) 012, arXiv:2207.01651.
- [38] J. Ghiglieri, M. Laine, *J. High Energy Phys.* 02 (2019) 014, arXiv:1811.01971.
- [39] B. Shuve, D. Tucker-Smith, *Phys. Rev. D* 101 (2020) 115023, arXiv:2004.00636.
- [40] J. Berman, B. Shuve, D. Tucker-Smith, *Phys. Rev. D* 105 (2022) 095027, arXiv:2201.11502.
- [41] T. Hambye, D. Teresi, *Phys. Rev. D* 96 (2017) 015031, arXiv:1705.00016.
- [42] S. Eijima, M. Shaposhnikov, I. Timiryasov, *J. High Energy Phys.* 07 (2019) 077, arXiv:1808.10833.
- [43] S. Eijima, M. Shaposhnikov, I. Timiryasov, *J. Cosmol. Astropart. Phys.* 11 (2017) 030, arXiv:1709.07834.
- [44] J.H. MacGibbon, B.R. Webber, *Phys. Rev. D* 41 (1990) 3052.
- [45] J.H. MacGibbon, *Phys. Rev. D* 44 (1991) 376.
- [46] A. Cheek, L. Heurtier, Y.F. Perez-Gonzalez, J. Turner, *Phys. Rev. D* 105 (2022) 015022, arXiv:2107.00013.
- [47] A. Cheek, L. Heurtier, Y.F. Perez-Gonzalez, J. Turner, *Phys. Rev. D* 106 (2022) 103012, arXiv:2207.09462.
- [48] B. Carr, K. Kohri, Y. Sendouda, J. Yokoyama, *Prog. Phys.* 84 (2020) 116902, arXiv:2002.12778.
- [49] R. Allahverdi, B. Dutta, K. Sinha, *Phys. Rev. D* 82 (2010) 035004, arXiv:1005.2804.
- [50] T.E. Oliphant, *A Guide to NumPy*, vol. 1, Trelgol Publishing, USA, 2006.
- [51] S. van der Walt, S.C. Colbert, G. Varoquaux, *Comput. Sci. Eng.* 13 (2011) 22.
- [52] P. Virtanen, R. Gommers, T.E. Oliphant, M. Haberland, T. Reddy, D. Cournapeau, et al., *Nat. Methods* 17 (2020) 261.
- [53] S.K. Lam, A. Pitrou, S. Seibert, in: Proceedings of the Second Workshop on the LLVM Compiler Infrastructure in HPC, 2015, p. 1.
- [54] W. Weckesser, odeintw: Complex and matrix differential equations, <https://github.com/WarrenWeckesser/odeintw>, 2014.
- [55] I. Esteban, M.C. Gonzalez-Garcia, M. Maltoni, T. Schwetz, A. Zhou, *J. High Energy Phys.* 09 (2020) 178, arXiv:2007.14792.
- [56] J.A. Casas, A. Ibarra, *Nucl. Phys. B* 618 (2001) 171, arXiv:hep-ph/0103065.
- [57] K. Nakamura, S.T. Petcov, in: M. Tanabashi, et al., Particle Data Group collaboration, *Phys. Rev. D* 98 (2018) 030001.
- [58] S.M. Bilenky, J. Hosek, S.T. Petcov, *Phys. Lett. B* 94 (1980) 495.
- [59] E. Molinaro, S.T. Petcov, *Eur. Phys. J. C* 61 (2009) 93, arXiv:0803.4120.